# Intruder-induced asymmetry in compartmentalized granular gases

Kuo-Ching Chen, Wen-Chin Li, and Wan-Lin Hsieh

*Institute of Applied Mechanics, National Taiwan University, Taipei 106, Taiwan, R.O.C.*

The clustering behavior of a compartmentalized monodisperse granular gas with the addition of one heavy intruding particle is investigated experimentally. Depending on the number of particles, the presence of a heavy intruder leads to three population states: a homogeneous state, an expelled clustering state, and a fully clustering state. These states are found to be consistent with the clustering of a purely monodisperse granular gas in an asymmetric compartmentalized structure. We obtain an exact relation between the size of an intruder and the elevation of the compartment bottom. This relation quantifies the particle-expelling ability of a heavy intruder, and suggests that the one-intruder system is a type of asymmetric system with an intruder-size-related asymmetrical index $\xi$. Under the framework of the flux model, a $\xi$-associated $\Xi$ function is proposed to quantitatively reproduce the experimental results.

## I. INTRODUCTION

The rich and complex phenomenon of a granular gas makes it become one of the paradigms for understanding nonlinear and nonequilibrium physics. Merely through inelastic collisions between grains and through the change of container geometry, bidisperse granular gases display diversity in their macroscopic behavior (especially in their mixing and separation) that usually goes beyond our understanding [1–4]. In compartmentalized systems [5–8], this diversity includes competitive clustering [9,10] and oscillatory clustering [11–16], relying on the driving condition and the number of particles.

The interaction between grains of the same species is seemingly simple. Adding one intruder into a monodisperse gas, however, could lead to a dramatic change in several physical properties of the whole system [17–20]. This can be exemplified by the change in the condensation temperature when one intruder is inserted into a monodisperse gas [21]. Through collisions, a heavier intruder transmits more kinetic energy to expel background grains, and on the contrary, a lighter intruder absorbs energy to trap the motion of grains. This expelling-trapping process illustrates the complex mechanism of granular oscillation [22,23]. Since a bidisperse granular gas can be viewed as a monodisperse gas with the addition of grains of other species, a closer scrutiny of a monosystem starting with few intruders and then with more intruders should be helpful to correctly predict the behavior intrinsic to a binary system.

It has been found that an intruder-fluid mixture behaves like a monodisperse gas in a container with a higher or lower barrier height [24]; however, the particle-expelling ability of an intruder has not yet been quantitatively explored. To this end, we perform a series of experiments to compare the particle population of a one-intruder system with that of an asymmetric one [25–27]. A one-intruder system refers to a monodisperse gas in a symmetric structure containing one intruder (cf. Fig. 2), while an asymmetric system indicates a monodisperse gas in an asymmetric structure (cf. Fig. 3). We witness three distinct states of particle distribution in two compartments for both systems as the total number of particles $N$ increases. They

are the homogeneous state, expelled clustering state (ECS), and fully clustering state (FCS). There is a clear difference between ECS and FCS, separated by a critical $N$, denoted as $N_{\mathrm{cr}}$. From the $N_{\mathrm{cr}}$ of each system, we will obtain for the first time a relation between the intruder size $d$ and the asymmetrical index $\xi$.

## II. EXPERIMENT

Our experimental apparatus consists of an electromagnetic shaker, which offers a vertically sinusoidal oscillation with dimensionless acceleration $\Gamma = (2\pi f)^2 a/g$, where $a$ is the shaking amplitude, $f$ is the frequency fixed at 20 Hz, and $g$ is the gravitational acceleration. On the top of the shaker we tightly mount an acrylic rectangular container $T_0$ of dimensions $W \times H \times D = 50 \times 150 \times 7.5\,\mathrm{mm}^3$ (where $W$ is the container width, $H$ the height, and $D$ the depth), which is divided into two equal compartments of width $w = 22.5\,\mathrm{mm}$ by an acrylic wall 5-mm thick. At a height $h = 40\,\mathrm{mm}$ above the compartment bottom, the wall has a rectangular opening of dimensions $S \times D = 2.5 \times 7.5\,\mathrm{mm}^2$ (where $S$ is the opening height). The stainless steel balls (mass density 7.92 g/cm$^3$) of diameter $d_B = 1\,\mathrm{mm}$ are adopted as the background particles, whose size allows them to pass through the opening. A larger steel ball of various diameters $d = 4 \sim 7\,\mathrm{mm}$ is used as the intruder, which is always confined in compartment L ($C_L$).

To explore the effect of a heavy intruder on the final distribution of background particles, we first adopt an intruder of diameter $d = 5\,\mathrm{mm}$ and randomly deposit the background particles of number $N$ within the two compartments as the initial condition. After subjecting these particles to a vertical shaking of $\Gamma = 8$ for 480 s, which is long enough to stabilize the particle population, we turn off the shaker and record the number of particles $N_L$ at $C_L$. By collecting all data for each $N$, the particle fraction at $C_L$, $\chi_L(=N_L/N)$, is plotted in Fig. 1, where the upward and downward arrows denote the directions of the system evolution. It can be found that all the particle systems for various initial depositions approach a certain steady state, indicated by the red dotted points. As shown in Fig. 1, there is a critical value of $N \approx 340$, above which two steady states (i.e., the upper and lower branches) are observed.
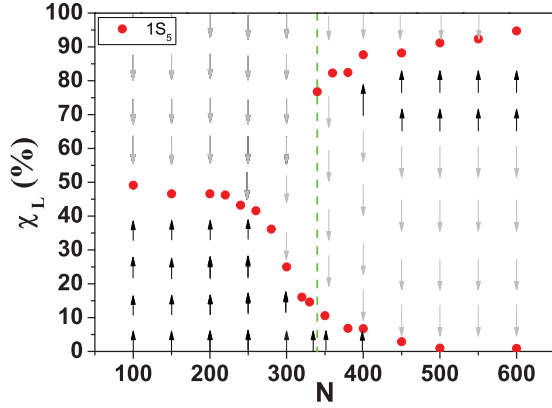
FIG. 1. (Color online) The particle fraction at $C_L$, $\chi_L$, versus the total number of particle $N$ for the one-intruder system, composed of the background particles of 1 mm and one heavy steel intruder of diameter $d = 5$ mm, denoted by the symbol $1S_5$. Initially all the particles are randomly placed within the two compartments, and then we count the number of particles at $C_L$ after 480-s oscillation of $\Gamma = 8.0$. The arrows represent the directions of the system evolution, and the red dotted points denote the final steady states.

In addition, Fig. 1 reveals that when $N < 200$, particles would distribute themselves uniformly between $C_L$ and compartment R ($C_R$), indicated by $\chi_L \approx 0.5$, and when $200 < N < 340$, most particles would cluster in $C_R$, indicated by $\chi_L < 0.5$.

According to the direction of the arrows in Fig. 1, we are able to obtain the critical $N$, called $N_{cr}$, one of the characteristics of the system, by simply performing the oscillation test under the initial condition of all particles being placed in $C_L$. This is because such an initial condition (i.e., beginning from $\chi_L = 1$ for all $N$) will lead to the steady states in the upper branch, and thus one can obtain $N_{cr}$ directly from the discontinuous curve formed by the red dotted points. Now, based on this specific initial condition and with the same driving condition as the previous test, we obtain the $\chi_L$-$N$ relation for each intruder diameter $d$, as shown in Fig. 2, which yields two findings. First, we observe that each curve with the same $d$ starts from about 50%, then drops to a minimum. For each $d$, the curve sharply jumps up at $N_{cr}$, and then smoothly approaches 100%. These features are distinguished by three stages. Stage I describes the uniform distribution when $N$ is small. As $N$ increases and $N < N_{cr}$, the gas goes into stage II, where the majority of particles are expelled by the intruder and condense in $C_R$. From this clustering pattern, we term it the expelled clustering state (ECS). In stage III, where $N > N_{cr}$, the initial deposition forces those particles to stay at $C_L$, resulting in most particles to cluster with the intruder. This is referred to as the fully clustering state (FCS). The second finding is that, if we denote the coordinates of the lower and upper jump points as $(N_{cr}, \chi^-)$ and $(N_{cr}, \chi^+)$ in Fig. 2, when $d$ increases, $N_{cr}$ increases, $\chi^-$ decreases, and $\chi^+$ roughly increases.

The same initial and driving conditions are then applied to an asymmetric-compartmentalized monodisperse system, where the asymmetry is made by elevating the compartment bottom of $C_L$ by $\Delta z$ (cf. Fig. 3). For this asymmetric system, an imperfect pitchfork bifurcation has been observed in the $\chi_L$-$v_b$ phase diagram [28], where the particle number $N$ is kept
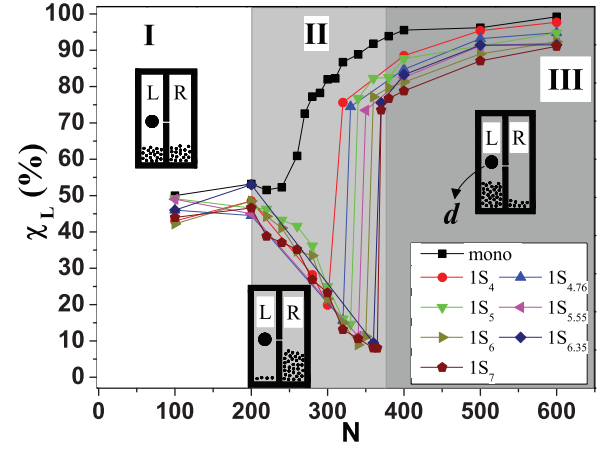


FIG. 2. (Color online) $\chi_L$ versus $N$ for the one-intruder system, composed of the background particles of 1 mm and one heavy steel intruder of diameter $d$ mm, denoted by the symbol $1S_d$. The initial condition is that all the particles are placed at $C_L$, and each data point is obtained by averaging 5 measurements of counting the number of particle at $C_L$ after 480-s oscillation of $\Gamma = 8.0$. Three stages of the distribution are observed as $N$ increases: particles are uniform (stage I), clustering away from the intruder (stage II), or clustering with the intruder (stage III). Stages II and III are separated by a critical number $N_{cr}$, which depends on the size of the intruder.

constant and $v_b (= af)$ is the shaker's driving velocity. Different from the $\chi_L$-$v_b$ relation, this work will explore the $\chi_L$-$N$ relation where $v_b$ is kept constant. We prepare six asymmetric containers with $\Delta z = 3 \sim 8$ mm, whose other dimensions are the same as the container $T_0$. This asymmetry is parameterized by the asymmetrical index $\xi$, which is defined as $\Delta z/h$. Figure 3 signifies the experimental similarity between the one-intruder and the asymmetric systems, where the variable of one intruder is changed into that of compartment bottom elevation. We also find three stages of particle population in the
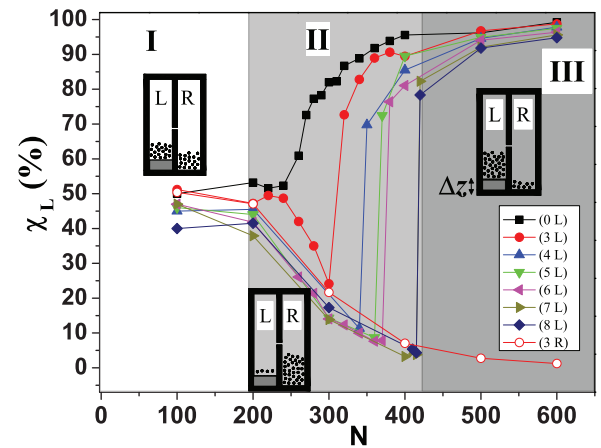


FIG. 3. (Color online) $\chi_L$ versus $N$ for monodisperse gases composed of particles of 1 mm in the asymmetric structure. Each data point is obtained with the same initial and driving conditions as in Fig. 2. Here in the symbol ($k$ L), "$k$" represents $\Delta z = k$ mm and "$L$" denotes that all particles are initially deposited at $C_L$. The feature of $\chi_L$ is similar to that in the one-intruder system. The only one case of initially placing the particles at $C_R$ is also illustrated, showing that the curve for (3 R) goes along the lower branch at stage III.
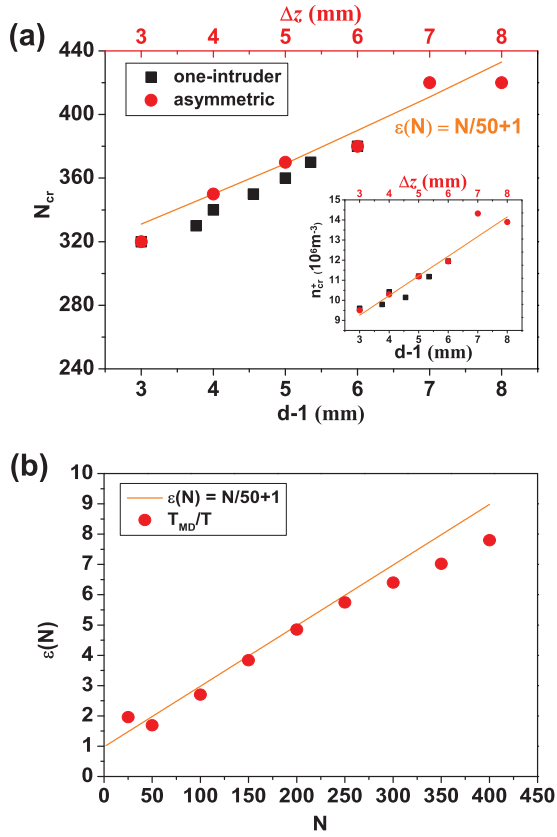
FIG. 4. (Color online) (a) The critical number $N_{cr}$ plotted against the intruder diameter (lower horizontal axis) for the one-intruder system and against the compartment bottom elevation (upper horizontal axis) for the asymmetric system. The solid line represents the theoretical $N_{cr}d$ relations obtained from the flux model, in which the parameter $\varepsilon$ is given by the relation $\varepsilon = (N/50) + 1$. Inset: The increasing tendency for the critical number density $n_{cr}^+$ at $C_L$ at the beginning of stage III. (b) An MD simulation result showing that $\varepsilon$ is a function of $N$. The data points are determined from the simulation, and the solid line with the equation $\varepsilon = (N/50) + 1$ is very close to these red points within the range of $25 < N < 400$.

asymmetric system. When $N$ is small, a uniform distribution is expected. As $N$ increases and $N < N_{cr}$, most particles cluster at $C_R$ (deep compartment); however, particles will cluster at $C_L$ (shallow compartment) when $N > N_{cr}$. It is found that a more shallow compartment (a larger $\Delta z$ and $\xi$) results in a larger $N_{cr}$, a smaller $\chi^-$, and a larger $\chi^+$.

As can be seen in Figs. 2 and 3, the same trend of $\chi_L$ versus $N$ implies that there is a one-to-one correspondence between the two systems. This can be explained by combining the plot of $N_{cr}$ versus $d$ and that of $N_{cr}$ versus $\Delta z$ in Fig. 4(a). The figure shows that when $(d - 1)$ and $\Delta z$ are used as the horizontal axis, both data for $N_{cr}$ in Figs. 2 and 3 seem to collapse into a straight curve-fitting line: $N_{cr} = a_1(d - 1) + b_1$ (or $N_{cr} = a_1\Delta z + b_1$), with $a_1 = 21.45$ and $b_1 = 255.59$. Since a larger $d$ (or $\Delta z$) causes a more violent motion for particles, we need more particles that increase collisions to suppress the violence, explaining the positive slope $a_1$. Accordingly, the parameter $a_1$ characterizes the increase of $N_{cr}$ as the intruder size (or $\Delta z$) increases, while the parameter $b_1$ represents the value of $N_{cr}$ for monodisperse gases composed of particles of 1 mm in a sym-

metric structure. Moreover, the limiting case of $d = d_B = 1$, which corresponds to $\Delta z = 0$, states that when the intruder is exactly the background particle, the one-intruder system degenerates to a symmetric one. Based on the $(d - 1)$ versus $\Delta z$ correspondence, it is plausible to propose the one-intruder system as an asymmetric one with the asymmetrical index $\xi$, which is expressed by

$$\xi = (d - d_B)/h, \qquad (1)$$

where $d_B = 1$ mm is adopted in this study.

The existence of this correspondence between the two systems does not imply that other macroscopic responses of the two systems are the same. In a system with an intruder, the intruder may transfer more transverse momentum to the small particles as compared to the asymmetric system. This indeed explains our observation that under the same initial condition (all particles deposited at $C_L$), the time to attain the steady state for particles in the one-intruder system, with the help of a higher transverse momentum by the intruder, is smaller than the time required in the asymmetric system. Thus, the correspondence represented by Eq. (1) is simply based on the two systems' similarly increasing trend of $N_{cr}$ when $d$ (or $\Delta z$) increases. This value of $N_{cr}$ is the minimum number above which most particles will not able to jump over the barrier; hence the $N_{cr}$ value generally reflects the total jumping ability of particles (i.e., a higher $N_{cr}$ corresponds to a higher jumping ability) of both systems.

Moreover, the inset of Fig. 4(a) shows the plot of the critical number density $n_{cr}^+$ versus $(d - 1)$ and $\Delta z$, where $n_{cr}^+ = N_{cr}\chi^+/V$ is the particle number per unit compartment volume at the beginning of stage III. Here $V = V_L - V_I$ is used for the one-intruder system and $V = V_L$ for the asymmetric system, with $V_L$ and $V_I$ being the volume of $C_L$ and that of the intruder, respectively. $n_{cr}^+$ can be realized as the critical number density in one compartment, beyond which particles will form a stable clustering therein.

### III. FLUX ANALYSIS

The $N_{cr}$-$d$ relation for the one-intruder system can be analytically predicted by using the phenomenological flux model [5,7,9]. In this model the flux function $F(N)$, characterizing the outflux from one compartment to another, takes the form $F(N) = (m/2\pi T)^{1/2}(gDSN/\Omega)\exp(-mgh/T)$ for a monodisperse system, where $N$, $m$, $T$, $D$, $S$, and $\Omega$, respectively, denote the particle number in that compartment, mass of one particle, granular temperature, container depth, opening height, and compartment ground area. When a system is composed of two species $i$ and $j$, the flux for species $i$ is extended to $F_i^{(2)}(N_i, N_j) = (m_i/2\pi T_i)^{1/2}(gDSN_i/\Omega)\exp(-m_igh/T_i)$, where each species has its own granular temperature $T_i$ which depends on both $N_i$ and $N_j$ [16]. Since the intruder at $C_L$ does not migrate to $C_R$, the correspondence of $(d - 1)$ versus $\Delta z$ allows us to replace the outflux of the background particles of number $N_i$ at $C_L$ in the one-intruder system with the outflux from $C_L$ in the corresponding asymmetric system, i.e., $F_{iL}^{(2)}(N_i, N_j; d) = F_L(N_i; h - \Delta z)$. Furthermore, the dynamical equilibrium for the particle inflow and outflow between $C_L$ and $C_R$ requires $F_{iL}^{(2)} = F_R$,

where $F_R$ is the outflux from $C_R$. Thus, we arrive at $F_L(N_L; h - \Delta z) = F_R(N_R; h)$, namely,

$$\frac{N_L}{\sqrt{T_L}} \exp\left[\frac{-mg(h - \Delta z)}{T_L}\right] = \frac{N_R}{\sqrt{T_R}} \exp\left(\frac{-mgh}{T_R}\right). \quad (2)$$

In Eq. (2), every quantity can be obtained from our direct measurement except the granular temperature $T_{L(R)}$. It can be determined by the balance of energy dissipation rate due to collisions and energy input rate from external oscillation within each compartment. By taking into account the particle-wall collisions in the energy input rate, this balance leads to [21,29]

$$T_{L(R)} = \alpha/(N_{L(R)} + \beta)^2, \quad (3)$$

where $\alpha = m(eaf\Omega)^2/[4\pi d^4(1-e)^2]$ and $\beta = \Omega/(\sqrt{2}\pi d^2)$. Here we assume that the coefficients of normal restitution for all collisions are the same, and will adopt $e = 0.9$ for simplicity. The correctness of Eq. (3) has been studied from a molecular dynamics (MD) simulation, showing that the mean kinetic energy of bidisperse granular gases is about 7 to 30 times higher than the theoretical value of $T$ [16]. In this study, we deal with this inconsistency, which comes from the simplicity inherent in this flux model, by simply modifying $T$ with an additional factor $\varepsilon$, i.e., $T = \varepsilon\alpha/(N + \beta)^2$. This factor can be further estimated by performing an MD simulation to simulate the actual average of kinetic energy of $N$ particles in a container. Our simulation adopts the soft-core MD code [30], and all of the parameters in this simulation, such as the container parameters (container's height), the particle parameters (mass, diameter of a background particle), and the shaking parameters are given as those used in our experiment. By taking the average of the recorded 50 000 sets of data within 50 s, we obtain the mean kinetic energy, denoted by $T_{\text{MD}}$, from which we obtain $\varepsilon = T_{\text{MD}}/T = T_{\text{MD}}/[\alpha/(N + \beta)^2]$ for different $N$. Figure 4(b) shows the $\varepsilon$-$N$ relation, where $\varepsilon$ is found to depend on the number of particles $N$ and this dependence can be approximated by a linear equation $\varepsilon = (N/50) + 1$ within the range of $25 < N < 400$.

In view of this modification, Eq. (2) reduces to

$$\Delta z = h - h\left(\frac{N - N_L + \beta}{N_L + \beta}\right)^2 - \frac{\varepsilon\alpha}{mg(N_L + \beta)^2} \ln\left[\frac{N_L(N_L + \beta)}{(N - N_L)(N - N_L + \beta)}\right]. \quad (4)$$

To analytically solve $N_L$, we nondimensionalize Eq. (4) by the length scale $h$ and propose a function $\Xi_N(x)$ as

$$\Xi_N(x) = \frac{(2x - N)(N + 2\beta)}{(x + \beta)^2} - \frac{\hat{\alpha}}{(x + \beta)^2} \ln\left[\frac{x(x + \beta)}{(N - x)(N - x + \beta)}\right], \quad (5)$$

where $x$ and $\hat{\alpha}$ stand for $N_L$ and $\varepsilon\alpha/(mgh)$, respectively. Since $\Xi_N(x)$ mathematically equals to $\Delta z/h$, it physically amounts to the asymmetrical index $\xi[= (d - d_B)/h]$ for the one-intruder system.

A quick glance at this function tells us that $\Xi_N(x) = 0$ if $x = N/2$, which indicates that a uniform distribution is an equilibrium state for a symmetric case ($\xi = 0$). Meanwhile,
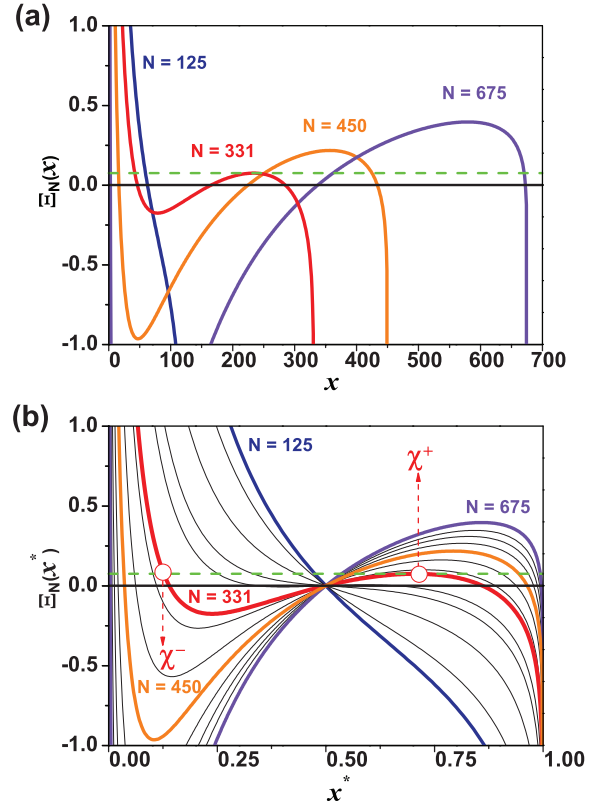
**(a)**

**(b)**

FIG. 5. (Color online) The analytical result from the flux model. (a) The function $\Xi_N(x)$ goes from positive infinity to negative infinity within the range of $0 \leqslant x \leqslant N$, and it intersects with the horizontal axis at one to three points depending on the $N$ number. (b) The diagram of $\Xi_N(x^*)$ with the horizontal axis rescaled as $x^*(=x/N)$. The shape of $\Xi_N(x^*)$ looks like a line going from $(0, +\infty)$, passing through $(1/2, 0)$, and to $(1, -\infty)$, twisted in a counterclockwise fashion, at the point $(1/2, 0)$. For a fixed $N$, $\Xi_N(x^*) = 3/40$ (indicated by the horizonal dashed green line) has one to three solutions.

we find that $\Xi_N(x) \to +\infty$ as $x \to 0^+$ and $\Xi_N(x) \to -\infty$ as $x \to N$. A close examination of $\Xi_N(x)$ by setting the values of $\hat{\alpha}$ and $\beta$ with our measurement reveals its features, as follows.

First, we see in Fig. 5(a) that when $N$ is small ($N < N_0$), $\Xi_N(x)$ is monotonically decreasing; however, when $N$ is large ($N > N_0$), $\Xi_N(x)$ has two extreme points, at which $d\Xi_N(x)/dx = 0$. Here, $N_0$ is the solution of $0 = d\Xi_N(x)/dx|_{x=N_0/2}$, and physically it is the total number of particles at which the bifurcation occurs for $\xi = 0$.

Second, let us consider the equation $\Xi_N(x) = 3/40$, which corresponds to $d = 4$ mm (or $\Delta z = 3$ mm). In Fig. 5(b), showing the enlarged plot around $\Xi_N(x^*) = 0$ with the horizontal axis rescaled as $x^*(=x/N = \chi_L)$, we observe that this equation has one to three solutions, depending on $N$. When $N < 331$, there is only one solution at $x^* = \chi_{L1}$ with $0 < \chi_{L1} < 0.5$; however, when $N > 331$, there are three solutions at $x^* = \chi_{L1}, \chi_{L2}, \chi_{L3}$ with $0 < \chi_{L1} < 0.5$ and $0.5 < \chi_{L2} < \chi_{L3} < 1$. For different $N$ we plot these solutions in Fig. 6, which displays the bifurcation nature and the three-stage distributions that resemble the experimental results in Figs. 2 and 3.

Third, when $N = 331$, $\Xi_N(x^*) = 3/40$ has two solutions at $x^* = \chi^-$ and $\chi^+$, with $0 < \chi^- < 0.5 < \chi^+ < 1$. The two solutions are the counterparts of the two points $(331, \chi^-)$ and
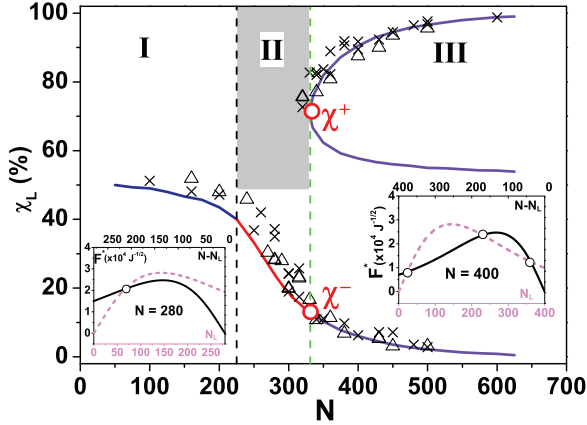
FIG. 6. (Color online) The analytical result from the flux model. The plot of the solutions $\chi_L$ of $\Xi_N(x^*) = 3/40$ vs $N$. The one-solution regime with $\chi_L \approx 0.5$, the regime with $\chi_L < 0.5$, and the three-solutions regime are, respectively, denoted as stages I, II, and III. The upper domain at stage II is called a "forbidden zone" since there is no solution within $0.5 < x^* < 1$. The symbols "$\triangle$" and "$\times$" respectively refer to the experimental data for $d = 4$ mm and $\Delta z = 3$ mm with random initial conditions. The two insets show the profiles of the flux-related function $F^* = [F(2\pi/m)^{1/2}(\Omega/gDS)]$ against $N_L$, pinpointing the solution(s) of $F_L^*(N_L) = F_R^*(N - N_L)$ in Eq. (1) when $\Delta z = 3$ mm for $N = 280$ and 400.

$(331, \chi^+)$ in the bifurcation diagram of Fig. 6. Therefore, we give $N_{cr} = 331$ for the case $d = 4$ mm (or $\Delta z = 3$ mm), which is close to our experimental data. The same procedure is applied to other values of $d$, generating the increasing relation between $N_{cr}$ and $d$, which is plotted in Fig. 4(a). Surprisingly, with the choice of $\varepsilon = (N/50) + 1$, the $N_{cr}$-$d$ relation is found to approximate our experimental data.

Fourth, the flux analysis offers all possible equilibrium states that are independent of the initial conditions; however, the majority of our previous experiments are limited by a given initial confinement. To check the consistency of our analysis and measurement, we further conduct many tests for a one-intruder system with $d = 4$ mm and an asymmetric system with $\Delta z = 3$ mm by randomly depositing particles at $C_L$ and $C_R$ at the beginning of each test. These outcomes fit well into the analytical curve, as shown in Fig. 6.

Fifth, we notice that within the range of $0.5 < x^* < 1$, there is no solution for $\Xi_N(x^*) = 3/40$ if $N < N_{cr}$. The null-solution region is characterized by the "forbidden zone" at stage II in Fig. 6, which indicates that it is never the case for most particles to condense at $C_L$ when $N < N_{cr}$, regardless of any initial conditions. This zone, which will degenerate as $\xi$ declines to zero, is a consequence of the symmetry breaking (or the intruder-induced asymmetry), resulting in a horizontal flow of most particles into a specific compartment.

Finally, our experiment reveals that no data point lies on the central branch at stage III. This is attributed to the condition of $d\Xi_N(x^*)/dx^*|_{x^*=\chi_2} > 0$, which requires that if $\chi_2$ and $\chi_2 + \delta\chi$ are the solutions of $\Xi_N(x^*) = 3/40$ and $\Xi_N(x^*) = [3 + \delta(\Delta z)]/40$, respectively, then the infinitesimal $\delta\chi$ and $\delta(\Delta z)$ obey $\delta\chi\delta(\Delta z) > 0$. This, however, contradicts our anticipation that to reach a new equilibrium state which slightly deviates from the original one, the more shallow $C_L$ is used $[\delta(\Delta z) > 0]$, the lower number of particles $N_L$ is expected ($\delta\chi < 0$). In short, $\delta\chi\delta(\Delta z) > 0$ would not exist.

## IV. CONCLUSION

We have demonstrated that the one-intruder system behaves like an asymmetric one with the asymmetrical index $\xi = (d - d_B)/h$. The index enables us to quantify the particle-expelling ability of one heavy intruder in a compartmentalized granular gas. We have found that the equilibrium states of particle distribution appear to bifurcate at a critical number of particle $N_{cr}$, which is shown to be an increasing function of $d$. Through the flux model analysis, we have associated the parameter $\xi$ with a proposed $\Xi$ function, which predicts all possible equilibrium states that are compatible with our observations. By manipulating the particle-expelling ability, i.e., by adjusting the intruder size, we aim to control and drive a unidirectional flow of background particles in a multicompartmentalized system. Future work will explore this issue in more detail.

[1] I. Goldhirsch and G. Zanetti, Phys. Rev. Lett. **70**, 1619 (1993).

[2] A. Barrat and E. Trizac, Mol. Phys. **101**, 1713 (2003).

[3] H. Hinrichsen and D. E. Wolf, *The Physics of Granular Media* (Wiley-VCH, New York, 2004).

[4] K. van der Weele, Contemp. Phys. **49**, 157 (2008).

[5] J. Eggers, Phys. Rev. Lett. **83**, 5322 (1999).

[6] J. J. Brey, F. Moreno, R. García-Rojo, and M. J. Ruiz-Montero, Phys. Rev. E **65**, 011305 (2001).

[7] K. van der Weele, D. van der Meer, M. Versluis, and D. Lohse, Europhys. Lett. **53**, 328 (2001).

[8] D. van der Meer, K. van der Weele, and D. Lohse, Phys. Rev. E **63**, 061304 (2001).

[9] R. Mikkelsen, D. van der Meer, K. van der Weele, and D. Lohse, Phys. Rev. Lett. **89**, 214301 (2002).

[10] R. Mikkelsen, D. van der Meer, K. van der Weele, and D. Lohse, Phys. Rev. E **70**, 061307 (2004).

[11] G. Costantini, D. Paolotti, C. Cattuto, and U. M. B. Marconi, Physica A **347**, 411 (2005).

[12] R. Lambiotte, J. M. Salazar, and L. Brenig, Phys. Lett. A **343**, 224 (2005).

[13] S. Viridi, M. Schmick, and M. Markus, Phys. Rev. E **74**, 041301 (2006).

[14] M. Hou, H. Tu, R. Liu, Y. Li, K. Lu, P. Y. Lai, and C. K. Chan, Phys. Rev. Lett. **100**, 068001 (2008).

[15] Y. Li, R. Liu, and M. Hou, Phys. Rev. Lett. **109**, 198001 (2012).

[16] K. C. Chen, C. H. Lin, and W. L. Hsieh, Phys. Rev. E **85**, 021306 (2012).

[17] A. Santos and J. W. Dufty, Phys. Rev. E **64**, 051305 (2001).

[18] A. Santos and J. W. Dufty, Phys. Rev. Lett. **97**, 058001 (2006).

[19] J. J. Brey, M. J. Ruiz-Montero, and F. Moreno, Phys. Rev. E **73**, 031301 (2006).

[20] V. Garzó and E. Trizac, Phys. Rev. E **85**, 011302 (2012).

[21] K. C. Chen, C. C. Li, C. H. Lin, and G. H. Guo, Phys. Rev. E **79**, 021307 (2009).

[22] K. C. Chen, C. C. Li, C. H. Lin, L. M. Ju, and C. S. Yeh, J. Phys. Soc. Jpn. **77**, 084403 (2008).

[23] K. C. Chen, C. H. Lin, C. C. Li, and J. J. Li, J. Phys. Soc. Jpn. **78**, 044401 (2009).

[24] K. C. Chen, W. L. Hsieh, and C. H. Lin, Phys. Rev. E **83**, 021303 (2011).

[25] M. Hou, Y. Li, R. Liu, Y. Zhang, and K. Lu, Phys. Status Solidi A **207**, 2739 (2010).

[26] Y. Li, M. Hou, and P. Evesque, J. Phys.: Conf. Ser. **327**, 012034 (2011).

[27] S. H. Shah, Y. Li, F. Cui, Q. Zhang, and M. Hou, Chin. Phys. B **21**, 014501 (2012).

[28] Y. Zhang, Y. Li, R. Liu, F. Cui, P. Evesque, and M. Hou, Chin. Phys. B **22**, 054701 (2013).

[29] Y. Li, R. Liu, M. Shinde, and M. Hou, Granular Matter **14**, 137 (2012).

[30] T. Pöschel and T. Schwager, *Computational Granular Dynamics: Models and Algorithms* (Springer, New York, 2005).